Chinese Chemical Letters 37 (2026) 110887

Contents lists available at ScienceDirect

Chinese Chemical Letters

journal homepage: www.elsevier.com/locate/cclet

Delicate pore environment regulation in pillar–layered metal–organic frameworks for enhanced C_2H_2/CO_2 separation

Nan Lu[a], Lan Lan[a], Qiang Gao[d,*], Ming Liu[a], Tong-Liang Hu[a], Na Li[b,c,*], Xian-He Bu[a,b]

[a] School of Materials Science and Engineering, Nankai University, Tianjin 300350, China
[b] State Key Laboratory of Elemento-Organic Chemistry, Frontiers Science Center for New Organic Matter, College of Chemistry, Nankai University, Tianjin 300071, China
[c] Haihe Laboratory of Sustainable Chemical Transformations, Tianjin 300192, China
[d] School of Environmental and Chemical Engineering, Jiangsu University of Science and Technology, Zhenjiang 212003, China

ARTICLE INFO

Article history:
Received 6 October 2024
Revised 14 January 2025
Accepted 19 January 2025
Available online 20 January 2025

Keywords:
Metal–organic framework
Pillar–layered strategy
Adsorption and separation
Pore environment regulation
C_2H_2/CO_2 separation

ABSTRACT

Controlling gas sorption *via* pore environment regulation is of significance yet challenging in the adsorption and separation process. Herein, we report a pillar modification strategy in the pillar–layered metal–organic frameworks for enhancing C_2H_2/CO_2 separation by controlling host-guest interactions. Altering pillars from aromatic ligand to aliphatic ligand in the prototype MOF (**Ni-MOF-1**) not only manufactures an aliphatic pore environment conducive to generate multiple van der Waals interactions with C_2H_2 but also increases adsorption sites for C_2H_2 verified by theoretical calculations. The pore environment optimized **Ni-MOF-2** exhibits 3.5-fold enhanced equimolar C_2H_2/CO_2 selectivity and practical separation performance evidenced by dynamic breakthrough experiments. This work provides an example for the in-depth investigation of delicate pore environment regulation and offers an alternative for the C_2H_2/CO_2 separation.

© 2026 Published by Elsevier B.V. on behalf of Chinese Chemical Society and Institute of Materia Medica, Chinese Academy of Medical Sciences.

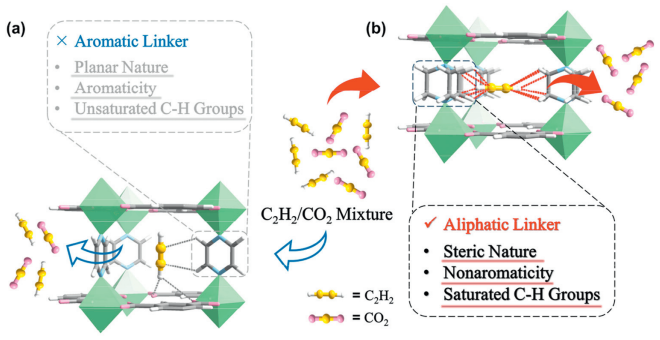
Acetylene (C_2H_2), as a key raw petrochemical material, is widely applied in manufacturing worthy chemical commodities such as acetaldehyde, acetic acid, and 1,4-butynediol [1–3]. However, carbon dioxide (CO_2) is the inevitable by-product of the acetylene industrial production process, and the existence of CO_2 will cut down energy conversion efficiency [4,5]. Owing to the identical molecular kinetic diameter and similar physical properties between CO_2 and C_2H_2 (Table S1 in Supporting information) [6–8], obtaining high-purity acetylene (>99 %) to manufacture valuable chemicals is relatively energy-intensive in the industry [9,10]. Consequently, developing energy-saving, cost-efficient, and environmentally friendly substitutive approaches is essential for C_2H_2 purification.

Porous physical adsorbents-based gas adsorptive separation can realize energy-efficient economy and operability, which has attracted the immense attention of researchers [11–13]. Metal–organic frameworks (MOFs) exhibit tunable pore structure, shape, and size [14], which provide numerous opportunities to create unique conditions for gas adsorption and separation. Pillar–layered MOFs (PL-MOFs) constructed from two-dimensional (2D) layers and adjustable pillars have great potential for C_2H_2 and CO_2 separation *via* delicate pore environment regulation [15–17]. To date, a pillar-layered strategy [18,19] utilizing the selection of different pillars with distinct chemical properties, has been applied in pore environment control of PL-MOFs to obtain the anticipatory pore environment for the optimization of C_2H_2/CO_2 separation [18]. Previous studies have proven that tuning the pillar length and derivatization is capable of manipulating the pore size and pore environment for task-specific gas separation [19,20]. However, most of the pillars are confined to aromatic linkers due to the characteristics of structural stability and easy functionalization [21]. Compared to aromatic linkers, aliphatic linkers possess desirable features such as steric effect, nonaromaticity, and saturated C–H groups [22,23], are expected to expand the kinds of MOF and conducive to create a low-polar pore chemical environment, which generates distinct host-guest interactions for distinguishing specific gas molecules [21,24,25]. So far, the study on the kind of host-guest interactions and the mechanism of adsorption between gas and aliphatic linkers are still scarce.

In light of these considerations, based on the tunability of PL-MOFs, we chose Ni(btc)(pyz) (named **Ni-MOF-1**; H_3btc = 1,3,5-benzene tricarboxylic acid; pyz = pyrazine) as a prototype MOF [26], which has verified the ability to remove trace CO_2 from C_2H_2/CO_2 mixture [27]. Inspired by abundant saturated C–H groups

* Corresponding authors.
E-mail addresses: gaoq@just.edu.cn (Q. Gao), lina@nankai.edu.cn (N. Li).

https://doi.org/10.1016/j.cclet.2025.110887
1001-8417/© 2026 Published by Elsevier B.V. on behalf of Chinese Chemical Society and Institute of Materia Medica, Chinese Academy of Medical Sciences.



Scheme 1. Depiction of the different C_2H_2 and CO_2 separation behavior in pillar–layered MOFs constructed by (a) aromatic and (b) aliphatic linkers.

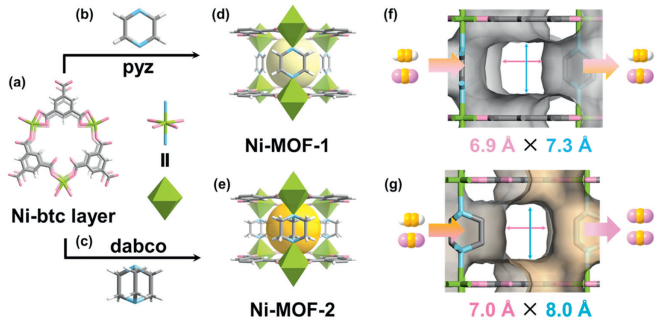


Fig. 1. The structural construction of **Ni-MOF-1** and **Ni-MOF-2** (Ni, green; C, gray; N, blue; O, pink; H, white; C_2H_2 and CO_2 are represented in space-filling models, C, yellow; O, pink; H, white). (a) 2D Ni-btc layer. (b, c) Pillars of pyz and dabco. (d, e) 3D PL-MOFs of **Ni-MOF-1** and **Ni-MOF-2**. Connolly surfaces of (f) **Ni-MOF-1** and (g) **Ni-MOF-2** with 1.0 Å of probes.

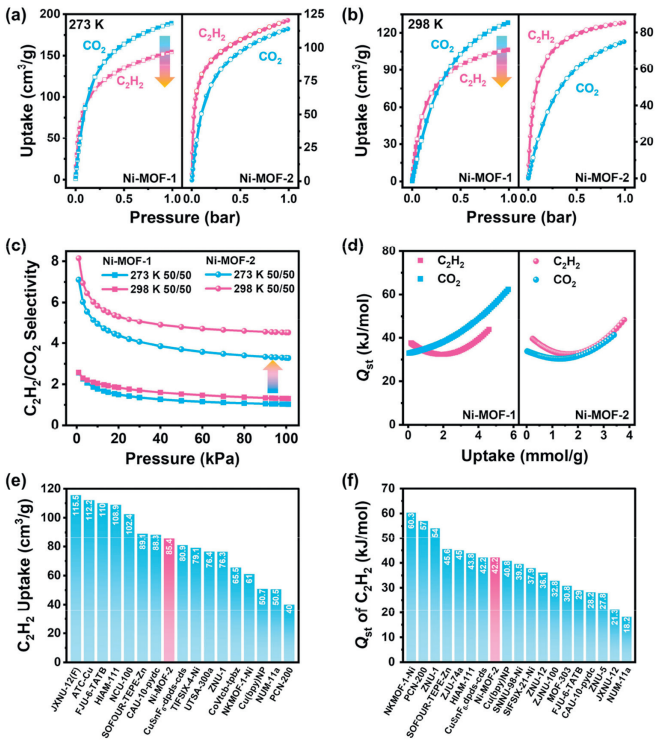


Fig. 2. C_2H_2 and CO_2 adsorption/desorption isotherms at (a) 273 K and (b) 298 K of **Ni-MOF-1** and **Ni-MOF-2**. (c) The equimolar C_2H_2/CO_2 separation selectivities of **Ni-MOF-1** and **Ni-MOF-2** at 273 K and 298 K. (d) The isosteric heat of adsorption of C_2H_2 and CO_2 for **Ni-MOF-1** and **Ni-MOF-2**. (e) Comparison of saturated C_2H_2 capacity at 298 K for **Ni-MOF-2** with those of other materials for C_2H_2/CO_2 separation. (f) Comparison of the zero-coverage isosteric heat of C_2H_2 for **Ni-MOF-2** with those of other materials for C_2H_2/CO_2 separation.

of the aliphatic ligand 1,4-diazabicyclo[2.2.2]octane (dabco), we speculate that tuning pillars from pyz to dabco may create an unusual aliphatic chemical environment, pore size, structural rigidity, and enhanced adsorption performance toward C_2H_2/CO_2 separation (Scheme 1) [25,28]. In this regard, Ni(btc)(dabco) (termed **Ni-MOF-2**) is successfully obtained based on reticular chemistry [29]. As expected, **Ni-MOF-2** not only exhibits the relatively high C_2H_2 capacity over CO_2 and 3.5-fold strengthened selectivity but also realizes a complete splitting of equimolar C_2H_2/CO_2 mixture (Scheme 1b). In addition, separation performance and regeneration stability for equimolar C_2H_2/CO_2 mixture of **Ni-MOF-2** were testified by the dynamic breakthrough experiments. Theoretical calculations reveal that host-guest interaction is converted from hydrogen bonding interaction to van der Waals (vdW) interaction and the saturated C–H groups of dabco serve as primary adsorption sites to interact with C_2H_2. The enhanced C_2H_2/CO_2 selectivity, low regeneration energy, and cyclic stability suggest that **Ni-MOF-2** is a promising porous adsorbent for C_2H_2/CO_2 separation.

Ni-MOF-1 and **Ni-MOF-2** are both obtained by the post-synthetic ligand exchange (PSLE) method [26,30,31]. They are two isostructural PL-MOFs constructed from the same 2D layers and different pillars (Figs. 1a–e). In the 2D layers, each Ni^{2+} ion coordinates with four O atoms from three btc ligands to form hexagon pores (Figs. S1 and S2 in Supporting information). Then, pyz and dabco as pillars (Figs. 1b and c) connect adjacent 2D layers (Fig. 1a) stacking up and down to generate three-dimensional (3D) frameworks of **Ni-MOF** with the same ***hms*** topology (Figs. 1d and e, Table S2 in Supporting information). **Ni-MOF-1** and **Ni-MOF-2** show hexagonal-prism cages with pore apertures of 6.9 Å × 7.3 Å [32] and 7.0 Å × 8.0 Å, respectively (Figs. 1f and g), which is consistent with pore size distribution (Fig. S7b in Supporting information). The high phase purity of **Ni-MOF-2** was verified by the bulk phase powder X-ray diffraction (PXRD) patterns (Fig S6 in Supporting information). The crystallinity of **Ni-MOF-2** can remain after being soaked in common organic solvents for 24 h (Fig. S8 in Supporting information). The whole structure and crystallinity of **Ni-MOF-2** survive up to 300 °C, as verified by thermogravimetric analysis (TGA) (Fig. S9b in Supporting information) and variable temperature PXRD (VT-PXRD) (Fig. S10 in Supporting information). Compared to the thermal stability of **Ni-MOF-1**, the thermal robustness of **Ni-MOF-2** is still preserved, implying the tiny impact of aliphatic pillars on the structural stability. The hexagonal-prism cages, chemical, and thermal stabilities of **Ni-MOF-2** pave the way for gas separation.

The activated **Ni-MOF-2** was prepared by heating at 150 °C for 12 h under a dynamic vacuum. Nitrogen (N_2) gas sorption isotherms at 77 K **Ni-MOF-2** show a typical type-I sorption curve, indicating the microporous structure of **Ni-MOF-2**. As shown in Fig. S7a (Supporting information), the saturated N_2 capacity of **Ni-MOF-2** increased from 282.4 cm^3/g [32] in **Ni-MOF-1** to 351.6 cm^3/g, aligning with the pore size derived from the single crystal structure. The calculated Brunauer–Emmett–Teller (BET) surface area of **Ni-MOF-2** is 636.0 m^2/g, slightly lower than the value of **Ni-MOF-1** (686.0 m^2/g) (Table S3 in Supporting information) [32]. Additionally, the effective free volume is also narrowed down from 52.8 % in **Ni-MOF-1** to 44 % in **Ni-MOF-2**. The microporosity, high porosity, appropriate pore size, and additional saturated C–H groups of **Ni-MOF-2** exhibit the potential to address the challenge of C_2H_2/CO_2 separation.

To verify the effect of pillar modification on the adsorption of gas molecules, single-component adsorption isotherms of $C_2H_2$and CO_2 for **Ni-MOF** were examined. As shown in Figs. 2a and b and

Fig. S11 (Supporting information), at both 273 K and 298 K, **Ni-MOF-1** prefers adsorbing C_2H_2 at low pressure but the higher CO_2 capacity upon increasing the pressure. However, after pillar variation of **Ni-MOF-1**, **Ni-MOF-2** demonstrates a higher C_2H_2 adsorption capacity than CO_2 within the full pressure region, indicating the potential of **Ni-MOF-2** for separating equimolar C_2H_2/CO_2. Moreover, for the diminution of surface area and effective free volume, the saturated capacities of C_2H_2 and CO_2 on **Ni-MOF-2** at 298 K are reduced from 106.4 cm^3/g and 128.2 cm^3/g to 85.4 cm^3/g and 75.1 cm^3/g, respectively (Fig. 2b and Table S3), demonstrating the greater reduction of CO_2 capacity and reversal of the interactions between frameworks and gas molecules after pore environment regulation. And the adsorption trend at 273 K of **Ni-MOF** is the same (Fig. 2a). Notably, the capacity of C_2H_2 of **Ni-MOF-2** at 298 K and 1 bar is higher than ZJU-74a (76.0 cm^3/g) [33], NKMOF-1-Ni (61.0 cm^3/g) [34], and Cu(bpy)NP (50.7 cm^3/g) [35], comparable to $CuSnF_6$-dpds-***cds*** (80.9 cm^3/g) [1], and CAU-10-pydc (88.3 cm^3/g) [36], and lower than NCU-100 (102.4 cm^3/g) [5], and HIAM-111 (108.9 cm^3/g) [37] under the same condition (Fig. 2e and Table S4 in Supporting information).

Subsequently, the ideal adsorbed solution theory (IAST) was employed to assess the adsorptive selectivity and evaluate the separation performance for equimolar C_2H_2/CO_2 mixture on **Ni-MOF-1** and **Ni-MOF-2**. As depicted in Fig. 2c, the equimolar C_2H_2/CO_2 selectivity of **Ni-MOF-1** is calculated as 1.0 and 1.3 at 273 K and 298 K and 100 kPa, respectively. Nevertheless, by virtue of switching pillars, **Ni-MOF-2** exhibits a relatively high selectivity of 3.3 and 4.5 for equimolar C_2H_2/CO_2 mixture, respectively, 3.3- and 3.5-fold higher than that of **Ni-MOF-1**, respectively, implying the enhanced separation potential of **Ni-MOF-2** for equimolar C_2H_2/CO_2. Meanwhile, the equimolar C_2H_2/CO_2 selectivity of **Ni-MOF-2** at 298 K outperforms that of some reported MOFs for C_2H_2/CO_2, such as SNNU-98-Ni (3.3) [38], HIAM-111 (2.4) [37], and FJU-90 (4.3) (Table S4) [39].

To compare the binding affinity of **Ni-MOF** toward C_2H_2 and CO_2, the isosteric heats of adsorption (Q_{st}) were calculated (Fig. S13 in Supporting information). For **Ni-MOF-1**, Q_{st} of C_2H_2 and CO_2 were calculated to be 38.6 kJ/mol and 32.8 kJ/mol at zero coverage, respectively (Fig. 2d). And the Q_{st} of C_2H_2 on **Ni-MOF-2** is 42.2 kJ/mol, surpassing the Q_{st} of CO_2 on **Ni-MOF-2** (32.2 kJ/mol) (Fig. 2d), exceeding that of ZNU-12 (36.1 kJ/mol) [2], and MOF-303 (30.8 kJ/mol) [36], inferior to SOFOUR-TEPE-Zn (45.6 kJ/mol) (Fig. 2f and Table S4) [8]. The appropriate Q_{st} of C_2H_2 facilitates regeneration using a low energy penalty. Increased adsorption disparity of C_2H_2 and CO_2, enhanced equimolar C_2H_2/CO_2 selectivity, and moderate isosteric heat of adsorption make **Ni-MOF-2** a prospective candidate for C_2H_2 purification.

To further validate the effect of pillar modification for equimolar C_2H_2/CO_2 separation, dynamic breakthrough experiments with different flow rates were conducted on **Ni-MOF-1** and **Ni-MOF-2** at 298 K and 1.0 bar. As shown in Figs. 3a and b, equimolar C_2H_2/CO_2 can be successfully separated on **Ni-MOF-2** with a total inlet flow rate of 1 and 2 mL/min, whereas **Ni-MOF-1** could not remove C_2H_2 from equimolar C_2H_2/CO_2 mixture. For **Ni-MOF-2** with a flow rate of 1 mL/min, CO_2 was first eluted through the column at 99.5 min/g, followed by C_2H_2 at 118.6 min/g (Fig. 3a). When the flow rates increased to 2 mL/min and 3 mL/min, **Ni-MOF-2** still achieved a clean separation of equimolar C_2H_2/CO_2 mixture, and the breakthrough point of CO_2 reduced to 53.6 min/g and 34.4 min/g (Figs. 3b and c). And **Ni-MOF-2** can be regenerated by purging argon. The separation performance and regeneration of **Ni-MOF-2** can be retained with a flow rate of 3 mL/min, proved by cycling breakthrough tests and PXRD (Fig. 3d and Fig. S17 in Supporting information). The practical separation performances and facile reproducibility pave the way for **Ni-MOF-2** as the available adsorbent to reduce the energy footprint.

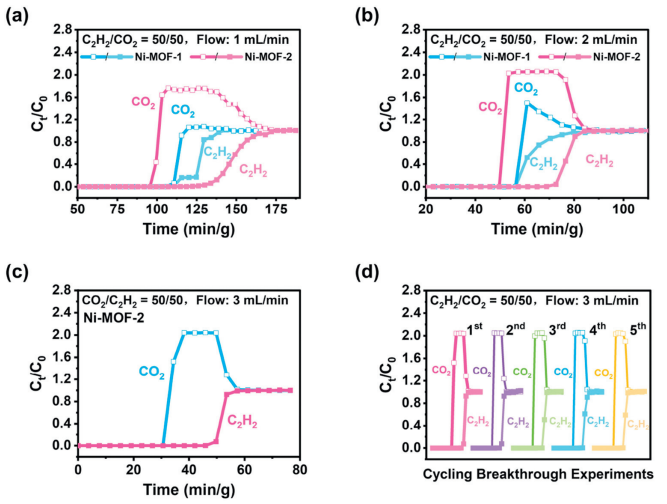


Fig. 3. Equimolar C_2H_2/CO_2 breakthrough curves of **Ni-MOF** at 298 K and 1.0 bar with a flow rate of (a) 1 mL/min and (b) 2 mL/min. (c, d) Cycling breakthrough tests of equimolar C_2H_2/CO_2 breakthrough curves of **Ni-MOF-2** at 298 K and 1.0 bar with a flow rate of 3 mL/min.

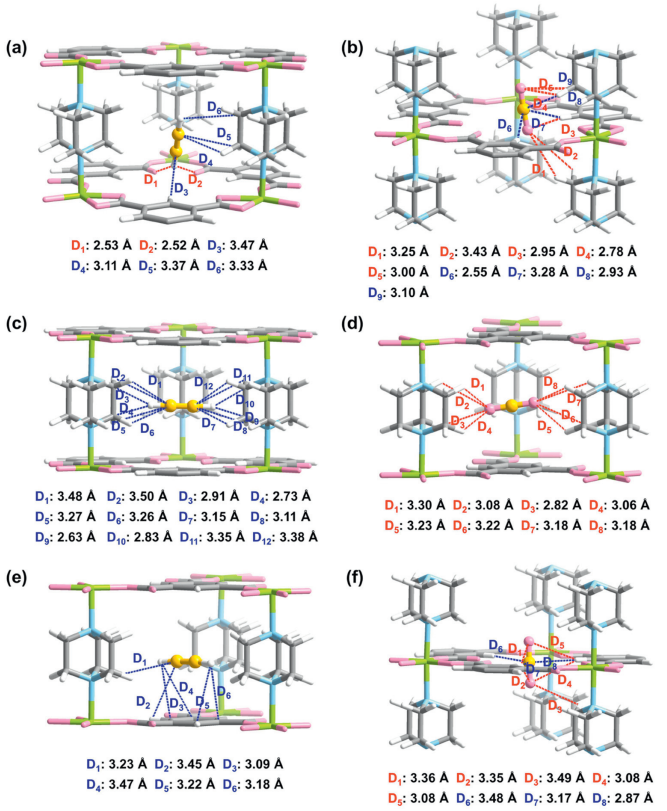


Fig. 4. DFT-calculated binding sites and interactions of C_2H_2 and CO_2 in **Ni-MOF-2** at (a, b) site I, (c, d) site II, and (e, f) site III. (a, c, e) C_2H_2, (b, d, f) CO_2 (Ni, green; C, gray; N, blue; O, pink; H, white; C_2H_2 and CO_2 are represented in ball-and-stick models, C, yellow; O, pink; H, white; The red dashed lines refer to C–H···O hydrogen bonding interactions; The blue dashed lines refer to C–H···C vdW interactions).

To elucidate the improved separation performance of **Ni-MOF-1** and **Ni-MOF-2**, grand canonical Monte Carlo (GCMC) simulations and density functional theory (DFT) calculations (Fig. 4) were performed on **Ni-MOF-2**. The aliphatic rings of btc ligands and saturated C–H groups of dabco ligands are the primary adsorption sites of C_2H_2 and CO_2 revealed by GCMC (Fig. S15 in Supporting information). As for DFT calculations, comparing with the C–H···O hydrogen bonding interactions as dominant host-guest interactions

between **Ni-MOF-1** and C_2H_2 or CO_2 [27], C–H···C vdW interactions and C–H···O hydrogen bonding interactions play the main role between frameworks and C_2H_2 and CO_2, respectively. As shown in Figs. 4a and b, after pillars regulation, in the site I of **Ni-MOF-2**, two C–H···O (H–O, 2.52–2.53 Å) hydrogen bonding interactions and four C–H···C (3.11–3.47 Å) vdW interactions between C_2H_2 and btc/dabco ligands were observed; as for CO_2, five C–H···O (H–O, 2.78–3.43 Å) hydrogen bonding interactions and four C–H···C (2.55–3.28 Å) vdW interactions were formed. In site II, C_2H_2 was firmly captured by twelve C–H···C (H–C, 2.63–3.50 Å) vdW interactions; however, eight C–H···O (H–O, 2.82–3.30 Å) hydrogen bonding interactions were formed between **Ni-MOF-2** and CO_2 (Figs. 4c and d, Table S5 in Supporting information). The binding pattern of site III is similar to site II (Figs. 4e and f, Table S5). The type of host-guest interactions of C_2H_2 underwent the variation from hydrogen bonding interaction to vdW interaction after pillar modification, invariable for CO_2; and the number of host-guest interactions plainly clarifies the reason for the improved separation performance of **Ni-MOF-2** compared with prototype **Ni-MOF-1**.

In summary, we reported two isostructural **Ni-MOF-1** and **Ni-MOF-2**, whose molecular recognition abilities for C_2H_2 and CO_2 are diverse. The challenge lies in equimolar C_2H_2/CO_2 mixture separation in **Ni-MOF-1** can be addressed *via* pillar variation from pyz to dabco by virtue of delicate pore environment regulation. Owing to supplemental vdW interactions with C_2H_2, pillar-modified **Ni-MOF-2** achieved efficient separation of equimolar C_2H_2/CO_2 and the 3.5-fold selectivity increased than that of **Ni-MOF-1**. The practical separation performance, cycle stability, and facile regeneration of **Ni-MOF-2** were validated by cyclic experimental breakthrough tests. DFT calculations proved that the extra C–H groups of dabco contribute to more C–H···C vdW interactions between C_2H_2 and the framework, guaranteeing preferential adsorption of C_2H_2 over CO_2 in **Ni-MOF-2**. This work sheds new light on delicate pore environment regulation for gas molecular recognition and suggests the potential for other challenging gas separations.

CRediT authorship contribution statement

Nan Lu: Writing – original draft, Visualization, Investigation, Formal analysis, Data curation. **Lan Lan:** Investigation, Formal analysis. **Qiang Gao:** Resources, Investigation, Formal analysis, Data curation. **Ming Liu:** Investigation, Funding acquisition, Formal analysis. **Tong-Liang Hu:** Visualization, Software, Formal analysis, Data curation. **Na Li:** Writing – review & editing, Supervision, Resources, Project administration, Funding acquisition, Formal analysis, Data curation. **Xian-He Bu:** Writing – review & editing, Supervision, Resources, Project administration, Funding acquisition.

Acknowledgments

This work was supported by the National Natural Science Foundation of China (Nos. 22035003, 22371139, 22305130), the Haihe Laboratory of Sustainable Chemical Transformations, and the Programme of Introducing Talents of Discipline to Universities (No. B18030).

Supplementary materials

Supplementary material associated with this article can be found, in the online version, at doi:10.1016/j.cclet.2025.110887.

References

[1] H. Xiong, Y. Peng, X. Liu, et al., Adv. Mater. 36 (2024) 2401693.
[2] Y. Zhang, Y. Han, B. Luan, et al., J. Am. Chem. Soc. 146 (2024) 17220–17229.
[3] Z. Zhang, Z. Deng, H.A. Evans, et al., J. Am. Chem. Soc. 145 (2023) 11643–11649.
[4] N. Kumar, S. Mukherjee, N.C. Harvey-Reid, et al., Chem 7 (2021) 3085–3098.
[5] J. Wang, Y. Zhang, Y. Su, et al., Nat. Commun. 13 (2022) 200.
[6] S.Q. Yang, T.L. Hu, Coord. Chem. Rev. 468 (2022) 214628.
[7] L. Wang, H. Huang, X. Zhang, et al., Coord. Chem. Rev. 484 (2023) 215111.
[8] X. Liu, P. Zhang, H. Xiong, et al., Adv. Mater. 35 (2023) 2210415.
[9] S.Q. Yang, R. Krishna, H. Chen, et al., J. Am. Chem. Soc. 145 (2023) 13901–13911.
[10] L. Zhang, K. Jiang, L. Yang, et al., Angew. Chem. Int. Ed. 60 (2021) 15995–16002.
[11] L. Li, R.B. Lin, R. Krishna, et al., Science 362 (2018) 443–446.
[12] X. Cui, K. Chen, H. Xing, et al., Science 353 (2016) 141–144.
[13] J.-B. Lin, T.T.T. Nguyen, R. Vaidhyanathan, et al., Science 374 (2021) 1464–1469.
[14] Y.P. Xia, C.X. Wang, M.H. Yu, et al., Chin. Chem. Lett. 32 (2021) 1153–1156.
[15] F. ZareKarizi, M. Joharian, A. Morsali, J. Mater. Chem. A 6 (2018) 19288–19329.
[16] X.L. Hu, F.H. Liu, H.N. Wang, et al., J. Mater. Chem. A 2 (2014) 14827–14834.
[17] X.L. Luo, Z. Yin, M.H. Zeng, et al., Inorg. Chem. Front. 3 (2016) 1208–1226.
[18] J. Qiao, X. Liu, X. Liu, et al., Inorg. Chem. Front. 7 (2020) 3500–3508.
[19] L. Liu, Z. Yao, Y. Ye, et al., J. Am. Chem. Soc. 142 (2020) 9258–9266.
[20] W. Li, J. Li, B. Zhang, et al., Chem. Eng. J. 483 (2024) 149126.
[21] J. Zhou, T. Ke, Y. Song, et al., J. Am. Chem. Soc. 144 (2022) 21417–21424.
[22] J. Zhou, K. Wen, T. Ke, et al., J. Am. Chem. Soc. 146 (2024) 16838–16847.
[23] C.S. Smoljan, Z. Li, H. Xie, et al., J. Am. Chem. Soc. 145 (2023) 6434–6441.
[24] J. Zhou, T. Ke, F. Steinke, et al., J. Am. Chem. Soc. 144 (2022) 14322–14329.
[25] B. Lal, K.B. Idrees, H. Xie, et al., Angew. Chem. Int. Ed. 62 (2023) e202219053.
[26] S. Jeong, D. Kim, S. Shin, et al., Chem. Mater. 26 (2014) 1711–1719.
[27] Y.Y. Liu, P. Zhang, W.Y. Yuan, et al., ACS Appl. Mater. Interfaces 16 (2024) 33451–33460.
[28] K.B. Idrees, Z. Chen, X. Zhang, et al., Chem. Mater. 32 (2020) 3776–3782.
[29] L. Shi, Z. Yang, F. Sha, et al., Sci. China Chem. 66 (2023) 3383–3397.
[30] P. Guo, M. Chang, T. Yan, et al., Chin. J. Chem. Eng. 42 (2022) 10–16.
[31] S. Jeong, D. Kim, X. Song, et al., Chem. Mater. 25 (2013) 1047–1054.
[32] N. Lu, L. Lan, Q. Gao, et al., Chem. Res. Chin. Univ. 40 (2024) 675–681.
[33] J. Pei, K. Shao, J.X. Wang, et al., Adv. Mater. 32 (2020) 1908275.
[34] Y.L. Peng, T. Pham, P. Li, et al., Angew. Chem. Int. Ed. 57 (2018) 10971–10975.
[35] Y. Liu, J. Liu, H. Xiong, et al., Nat. Commun. 13 (2022) 5515.
[36] S.M. Jeong, D. Kim, J.Y. Park, et al., ACS Appl. Mater. Interfaces 16 (2023) 1342–1350.
[37] J. Miao, W. Graham, J. Liu, et al., J. Am. Chem. Soc. 146 (2024) 84–88.
[38] J.W. Wang, S.C. Fan, H.P. Li, et al., Angew. Chem. Int. Ed. 62 (2023) e202217839.
[39] Y. Ye, Z. Ma, R.B. Lin, et al., J. Am. Chem. Soc. 141 (2019) 4130–4136.